coatings

MDPI

Article

# S-Layer Protein Coated Carbon Nanotubes

**Andreas Breitwieser [1], Philipp Siedlaczek [2], Helga Lichtenegger [2], Uwe B. Sleytr [1] and Dietmar Pum [1,*]**

[1] Department of Nanobiotechnology, Institute of Biophysics, University of Natural Resources and Life Sciences Vienna, Muthgasse 11, 1190 Vienna, Austria

[2] Department of Material Sciences and Process Engineering, Institute of Physics and Materials Science, University of Natural Resources and Life Sciences Vienna, Peter-Jordan-Straße 82, 1190 Vienna, Austria

* Correspondence: dietmar.pum@boku.ac.at; Tel.: +43-47654-80360

Received: 16 July 2019; Accepted: 31 July 2019; Published: 2 August 2019




**Abstract:** Carbon nanotubes (CNTs) have already been considered for medical applications due to their small diameter and ability to penetrate cells and tissues. However, since CNTs are chemically inert and non-dispersible in water, they have to be chemically functionalized or coated with biomolecules to carry payloads or interact with the environment. Proteins, although often only randomly bound to the CNT surface, are preferred because they provide a better biocompatibility and present functional groups for binding additional molecules. A new approach to functionalize CNTs with a closed and precisely ordered protein layer is offered by bacterial surface layer (S-layer) proteins, which have already attracted much attention in the functionalization of surfaces. We could demonstrate that bacterial S-layer proteins (SbpA of *Lysinibacillus sphaericus* CCM 2177 and the recombinant fusion protein rSbpA$_{31\text{-}1068}$GG comprising the S-layer protein and two copies of the IgG binding region of Protein G) can be used to disperse and functionalize oxidized multi walled CNTs. Following a simple protocol, a complete surface coverage with a long-range crystalline S-layer lattice can be obtained. When rSbpA$_{31\text{-}1068}$GG was used for coating, the introduced functionality could be confirmed by binding gold labeled antibodies via the IgG binding domain of the fusion protein. Since a great variety of functional S-layer fusion proteins has already been described, our new technology has the potential for a broad spectrum of functionalized CNTs.

**Keywords:** S-layer protein; carbon nanotubes; functionalization; non-covalent; IgG binding domain; dispersion; aqueous solution

## 1. Introduction

Since their discovery, carbon nanotubes (CNTs) have already been intensively investigated and characterized in material sciences due to their outstanding mechanical, electrical, and thermal properties [1–4]. While some of the developments of new applications are still in progress, others have already been materialized into new products. Moreover, CNTs have also been considered for several medical applications due to their small diameter and ability to penetrate cells and tissues [5]. However, since pristine CNTs are chemically inert and not dispersible in water or organic solvents, they have to be functionalized or modified to carry payloads or interact with the environment [6–11].

Proteins bound to the surface of CNTs are preferred in life-sciences because they provide a better biocompatibility and offer functional groups that may either be used for binding additional molecules in biosensor applications [12–19] or enable further chemical modifications, e.g., for the delivery of drugs, DNA and genes [20,21]. Nevertheless, although several proteins, such as bovine serum albumin (BSA), have already been successfully attached to CNTs through various physical or chemical methods, high resolution microscopical studies have demonstrated that their arrangement and density on the CNT surface and consequently the availability of functional groups varies considerably [5].

An alternative and better controlled approach to functionalize CNTs with an additionally closed and precisely ordered protein layer is offered by bacterial surface layer (S-layer) proteins which have already attracted much attention in the functionalization of surfaces as well as supporting structures for biomembranes [22–25].

S-layer proteins are one of the most abundant biopolymers on earth and form the outermost cell envelope component in a broad range of bacteria and archaea (Figure 1a) [22]. In addition to the surface of bacterial cells, S-layer proteins have the natural capability to reassemble into crystalline monomolecular arrays on solid supports, at the air-water interface, planar lipid films, liposomes, emulsomes, nanocapsules, and nanoparticles (Figure 1b) [23].

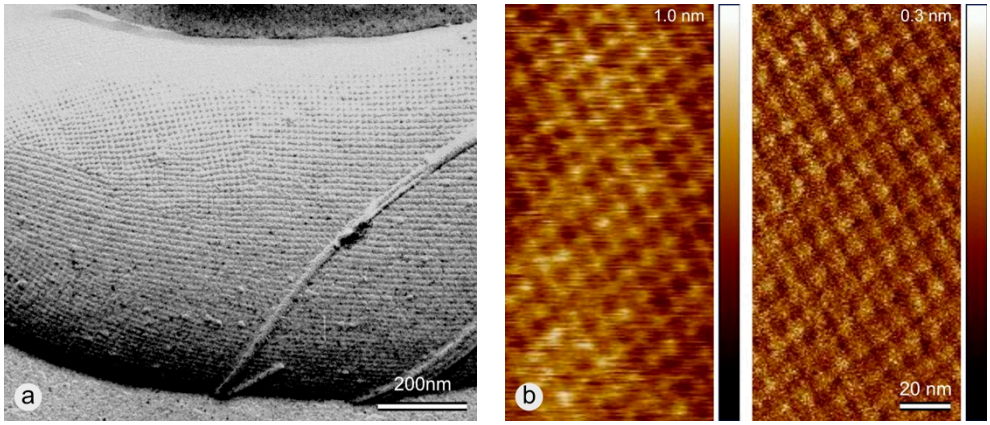



**Figure 1.** (**a**) TEM micrograph of a freeze-etched and metal shadowed preparation of a bacterial cell of *Lysinibacillus sphaericus* CCM 2177 with an S-layer as the outermost cell envelope component. The numerous lattice faults are a consequence of the bending of the S-layer lattice at the rounded cell poles. In addition, the rope-like structures are the flagella of the bacterial cell. (Reproduced from Reference [26] with permission from the Royal Society of Chemistry.) (**b**) AFM images of a monolayer of the SbpA S-layer lattice of *Lysinibacillus sphaericus* CCM 2177 on a silicon wafer. (Height image (left) and deflection error image (right)). The S-layer lattice shows square lattice symmetry. Unit cell size is 13.1 × 13.1.

S-layers are isoporous protein mesh works with unit cell sizes in the range of 3 to 30 nm, thicknesses of 5 to 10 nm (up to 70 nm in archaea), and pore sizes of 2 to 8 nm (Figure 1b). Since S-layers are composed of a single protein or glyco-protein species they may be considered as the simplest biological membranes developed in the course of evolution.

In particular, the formation of monolayers on technologically important substrates, such as silicon or glass, was always a major concern for the development of affinity matrices, biosensing layers or the development of organic-inorganic hybrid architectures [24,27]. In this context, it was seen as a further challenge to investigate the reassembly of S-layer proteins on CNTs and learn from nature how these new hybrid architectures may be used to develop a possible next generation of biological sensing layers. Key to such developments are S-layer (fusion) proteins [22,28] that, on the one hand, have retained the natural self-assembly properties of the wild-type proteins and, on the other hand, are endowed with particularly tailored bio-reactive domains that allow a highly specific and sensitive functionalization of surfaces. As a matter of fact, functional groups on the protein lattice are arranged in well-defined positions and orientations [22,24]. Examples are affinity matrices with S-layer fusion proteins carrying the immunoglobulin G (IgG) binding domains of Protein A or Protein G [29–31] or the green fluorescent protein (GFP and its variants) for Förster- or Fluorescence-energy transfer (FRET) pairs in DNA-hairpin sensors [32]. In this context, it has to be stressed that the high binding capacity of S-layer proteins would also be retained after intra- and intermolecular crosslinking (e.g., by glutardialdehyde or Dimethyl-pimelimidatedihydrochloride (DMP)). It has been shown that cross-linking enhances the

mechanical and chemical stability of S-layers (e.g., at sudden pH changes or higher temperatures) considerably [24].

To our knowledge, this work describes for the first time the reassembly of an S-layer protein; in particular, of SbpA, the S-layer protein from *Lysinibacillus sphaericus* CCM 2177 [33,34] (identical to *Lysinibacillus sphaercius* ATCC 4525, see Reference [35]) with its characteristic square (p4) lattice symmetry on CNTs. With respect to the unit cell size of SbpA with 13.1 × 13.1 nm, we decided to work with multiwalled nanotubes (MWNTs) with diameters ranging from 50–90 nm since the diameters of single- and double-walled nanotubes (typically below 10 nm) might be too small (Figure 2). The addition of S-layer protein to aggregated CNTs led to an instantaneous dispersion of the CNTs. According to the literature, amphiphilic molecules, such as S-layer proteins, are suitable to disperse CNTs in water by shielding their highly hydrophobic surface [8,36]. Moreover, we assume that this effect might be emphasized by the fact that S-layer recrystallization follows a two-step non-classical reassembly process [37–39] in which the adsorption process is instantaneously completed and followed by a subsequent slower transition from the amorphous to the crystalline phase in the presence of calcium ions only [39–42].

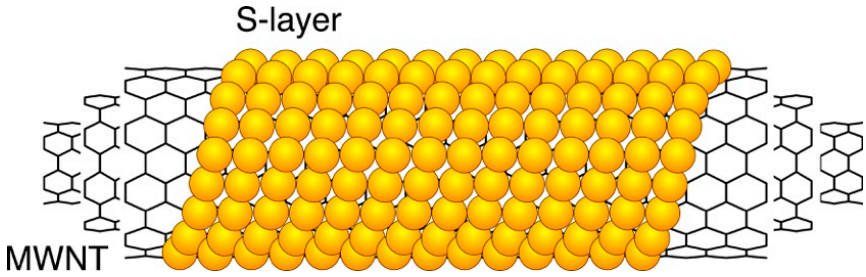



**Figure 2.** Schematic drawing of an S-layer coated multi walled carbon nanotube.

Finally, preliminary experiments with rSbpA$_{31\text{-}1068}$GG fusion protein and binding of colloidal gold labeled antibodies did not only give information about the orientation of the S-layer proteins bound on the carbon nanotubes but also about the functionality of the so coated and functionalized hybrid structures [29,30].

## 2. Materials and Methods

### *2.1. Production of Wild Type and Recombinant S-Layer Fusion Protein Solutions*

*L. sphaericus* CCM 2177 (from the Czech Collection of Microorganisms) was grown in continuous culture as described in a previous study [43]. Cell wall fragments were obtained after a downstream process and used as starting point for the production of a monomeric wild type SbpA (wtSbpA) S-layer protein solution [44]. The protein was extracted with 5M guanidine hydrochloride (GHCL, Gerbu Nr. 1057) and after centrifugation dialyzed (membrane Biomol cut-off: 12–16 kD; pore size 2.5 nm) against 3 L Milli-Q water containing 2 mM ethylenediaminetetraacetic acid (EDTA). The resulting protein solution was adjusted to a final concentration of 1 mg/mL. The reassembly properties of the so obtained monomeric protein solution were determined by atomic force microscopy (AFM) (Multimode AFM, Bruker AXS, Santa Barbara, CA, USA) [45]. For this purpose, the protein solution was diluted with a crystallization buffer containing $CaCl_2$ to a final concentration of 100 µg/mL and applied on 10 × 10 mm sized silicon wafer pieces [39]. Only when the SbpA S-layer lattice with its characteristic square lattice symmetry could be visualized by AFM (Figure 1b), the protein solution was used for the experimental work and stored at 4 °C for a maximum of 4 weeks.

The S-layer fusion protein rSbpA$_{31\text{-}1068}$GG comprising a truncated—but still reassembly capable—form of SbpA with two IgG binding regions cloned from Protein G was expressed and purified as described in Reference [30]. The resulting monomeric protein solution was adjusted to

a concentration of 1 mg/mL, the reassembly capability controlled by AFM, and stored as described above for the wtSbpA protein solution.

### *2.2. Coating of -COOH Functionalized MWNTs with S-Layer Proteins*

In order to enhance the dispersion of multiwalled nanotubes (MWNTs) in aqueous buffer solutions carboxyl groups (-COOH) were introduced by oxidation following the protocol of Singer et al. in Reference [46]. Here, pristine MWNTs (SIGMA, Saint Louis, MO, USA; diameter of 50–90 nm, Nr. 901019) were suspended in 30% $H_2O_2$ (Roth, Nr. 8070) stirred and heated in an oil bath at 130 °C for a total of 4 h. After a filtration and washing step, the functionalized MWNTs were dried at 70 °C for 48 h.

These -COOH functionalized MWNTs were suspended in crystallization buffer (4 mg/30 mL; 5 mM Tris and 100 mM $CaCl_2$ in Milli-Q water, pH 9.0) under the aid of ultrasonication (Branson Sonifier 250; output 5, duty circle 50%) for 20 min. From this, still not well dispersed, solution 4.5 mL were transferred into a container with 500 µL wtSbpA or rSbpA$_{31\text{-}1068}$GG monomeric protein solution (1 mg/mL) and ultrasonication was prolonged immediately for 4 min. This step was carried out in an ice bath to avoid possible denaturation of the S-layer protein caused by raising temperatures (typically > 45 °C) during ultrasonication. Subsequently, incubation was allowed to take place overnight at 4 °C using an overhead shaker (Heidolph, Reax 2, Schwabach, Germany). After 16 h the S-layer coated MWNTs were centrifuged (Eppendorf; Centrifuge 5424, Hamburg, Germany) at 5000 rcf for 10 min and resuspended in crystallization buffer to a final concentration of 1 mg/mL.

### *2.3. Immuno Gold Labeling of rSbpA$_{31\text{-}1068}$GG Coated -COOH Functionalized MWNTs*

From rSbpA$_{31\text{-}1068}$GG coated MWNTs suspension 500 µL were centrifuged (Eppendorf; Centrifuge 5424) at 5000 rcf for 5 min, resuspended and incubated with gold labeled goat anti-human IgG (Amersham, AuroProbe$^{TM}$BL plus, RPN 464F) 1:5 diluted in crystallization buffer (pH 9.0) containing 0.01% Triton-X 100 and 0.001% fish gelatin (Amersham, RPN 416V) at RT for 3 h. Goat IgG binds via the IgG binding moieties of the fusion protein. Subsequently, labeled MWNTs were washed once with crystallization buffer (centrifugation step: 5000 rcf for 10 min), negative stained, and investigated by transmission electron microscopy (TEM).

### *2.4. Transmission Electron Microscopy (TEM), Negative Staining, and Image Processing*

The ability of S-layer proteins to form a crystalline and in the case of rSbpA$_{31\text{-}1068}$GG a biologically active coating on MWNTs was demonstrated with an FEI Tecnai T20 Transmission Electron Microscope (TEM) operated at 160 kV (FEI Europe (now ThermoScientific), Eindhoven, The Netherlands) after negative staining of the samples. For this purpose, samples were adsorbed on 300 mesh copper grids (Christine Gröpl Elektronenmikroskopie, Tulln, Austria) coated with a Formvar-support film and a thin carbon layer. A chemical fixation of the protein adsorbed on the copper grids was done with a drop of 2.5% glutaraldehyde in cacodylate buffer (pH 7.4) for 10 min. For negative staining, samples were place on 2% uranium acetate drops for 10 min. All steps were performed at room temperature. The open source software ImageJ (version 1.52p) was used to straigthen bent S-layer coated MWNTs in TEM images and subsequently to calculate the Fourier spectrum showing the layer lines of the helical S-layer [47].

### *2.5. Preparation of Bucky Paper and Scanning Electron Microscopy*

Buckypapers are simple membrane based CNT architectures [48]. In this study, buckypapers were prepared by filtration of wtSbpA coated MWNTs using an AMICON filtration unit (AMICON, Burlington, MA, USA; ultrafiltration cell Model 8010). A micro-filter (SARTORIUS, Goettingen, Germany; Sartolon polyamide, Nr. 25007-47-N) with a pore size of 0.2 µm was chosen as supporting membrane. After deposition of the S-layer functionalized MWNTs on the membrane surface, the buckpaper was removed from the filtration cell, air-dried and characterized with a ThermoScientific Apreo VS SEM (ThermoScientific, Eindhoven, The Netherlands) scanning electron microscope (SEM).

For this purpose, the bucky paper was cut into approx. 5 × 5 mm sized pieces and fixed with a conductive double sticky tape on standard 0.5″ aluminum stubs. The SEM was operated at 2.0 kV with a beam current of 0.1 nA in immersion (high resolution) mode. Images were recorded in high vacuum with the in-lens back-scattered electron (BSE) detector T1 and the secondary electron (SE) detector T2.

## 3. Results

### *3.1. Bucky Paper*

Bucky paper was produced in order to make a quick check of the supplied MWNT diameters. The diameters were measured in the SEM images (n = 70) and found to be within the 50–90 nm range given by the manufacturer (70.1 ± 14.8nm; min = 43; max = 106 nm) (Figure 3). The bright areas in Figure 3b show the charging of the electrically insulating polymeric microfilter.

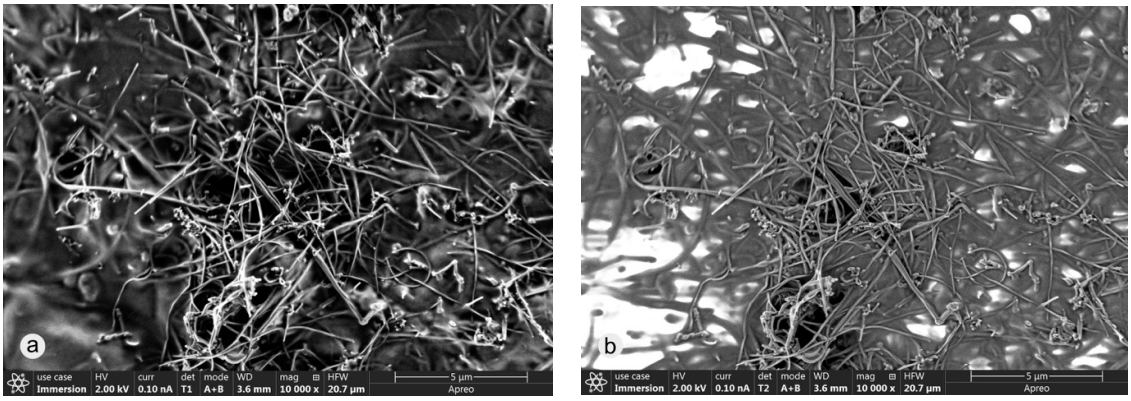



**Figure 3.** Bucky paper imaged in the SEM with the (**a**) BSE detector (T1) and the (**b**) SE detector (T2) detector. Note the difference between the material and topography contrast provided by the back-scattered and secondary electrons, respectively. Moreover, the pores in the microfiltration membrane are clearly visible in (**b**).

### *3.2. Coating of -COOH Functionalized MWNTs with wtSbpA S-Layer Protein*

It was clear right from the beginning that a homogeneous dispersion of the MWNTs is absolutely necessary for the investigation and technological application of a successful S-layer coating. According to the literature, the MWNTs could not be easily dispersed in aqueous buffer solution even after oxidation with the associated introduction of -COOH groups and subsequent ultrasonication. This inhomogeneous suspension was not suitable for a successful S-layer coating, but when wtSbpA S-layer protein was added and ultrasonication prolonged, the suspension became immediately homogeneous (Figure 4). The suspension was stable then for at least several months (since the commencement of the work) and when required only had to be shaken in order to resuspend the sedimented S-layer coated MWNTs again.

It was assumed that the amphiphilic SbpA S-layer proteins were instantaneously attached to the MWNT surface and in this way shielded the highly hydrophobic MWNT surfaces from the aqueous medium. S-layer reassembly follows a two-stage non-classical pathway in which first extended monomers are attached to the surface, form amorphous and subsequently microcrystalline clusters from which crystalline order emerges by a final folding step. Calcium ions play an important role for the reassembly of most S-layer proteins including SbpA [39–42]. TEM investigations demonstrated that the S-layer completely covers the -COOH functionalized MWNTs (Figure 5).

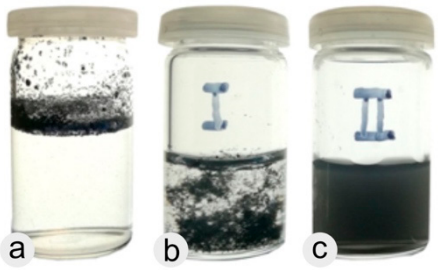



**Figure 4.** Different MWNT suspensions after various consecutive treatments. (**a**) Resuspension of pristine MWNTs in recrystallization buffer. (**b**) Sample I: -COOH functionalized MWNTs in recrystallization buffer after ultrasonication (20 min). (**c**) Sample II: further treatment of sample I by adding wtSbpA S-layer protein in the course of a second short (4 min) ultrasonication step.

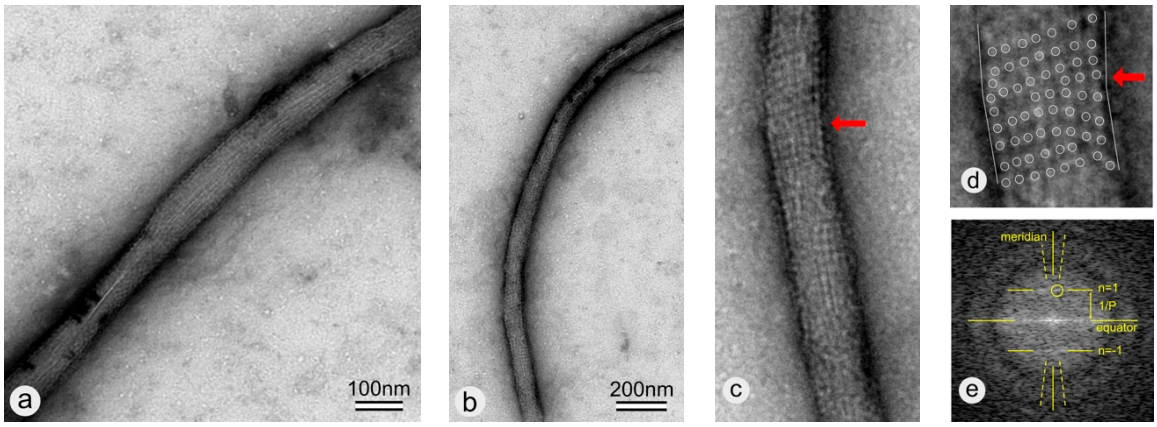



**Figure 5.** (**a**,**b**) TEM images of negatively stained wtSbpA coated MWNTs. The wtSbpA coating exhibits a crystalline lattice with square lattice symmetry. (**c**) Zoomed view of the lower end of the S-layer coated MWNT shown in (**b**). Note the lattice defect in the S-layer lattice (marked by the red arrow) where the MWNT buckles in (**c**) and in the further zoomed view in (**d**) where the unit cell positions are marked by circles too. (**e**) Fourier spectrum of a straightened copy of (**c**) showing the layer lines n = ±1 and in this way the corresponding pitch P of the helical S-layer.

A highly ordered protein layer exhibiting square lattice symmetry can be clearly seen, confirming the ability of wtSbpA to reassemble on -COOH functionalized MWNTs over long (several tens of micrometer) distances (Figure 6a). Lattice defects in the S-layer lattice, in particular disclinations, were found where the MWNT buckles (Figure 5c,d) [49]. Moreover and in general, the TEM image shows a side-on-view (elevation) of a helix with an axial repeat, termed pitch P. Thus, the Fourier spectrum will have an axial repeat along the Z-axis (the meridian) of 1/P. This generates a set of equally spaced layer lines separated by 1/P and indexed from Z = 0 (the equator) with n = 0, 1, 2, . . . in the Z-direction and by negative integers in the –Z-direction. The amplitudes of the diffraction orders along a particular layer line are proportional to Bessel functions $J_n$ of order n [50]. Because only $J_0$ is non-zero on the Z-axis, only the n = 0 layer line will be non-zero on the meridian. Successive first maxima of $J_n$ progressively occur further from the Z-axis giving the appearance of a cross-characteristic for the Fourier spectrum of a helix- with intensities decreasing as n increases. In the Fourier spectrum (Figure 5e), only the first maximum in the first layer lines (n = ±1) is visible. The value of 1/P was determined with 1/13.67 nm which led us to the conclusion that the S-layer proteins with their unit cell size of 13.1 nm were arranged along a single basic helix or, in other words, that the helical repeat consisted of only one striation. The pitch angle was determined to be approximately 6.5°. For a more detailed description of how to analyze and index a diffraction pattern of a helical structure, see Reference [51]. Moreover, it has to be mentioned that the S-layer coating did not close the MWNT ends. This finding was not surprising since only S-layer proteins which reassemble in hexagonal (p6) lattice symmetry would be

able to make rounded caps or closed vesicles [25] by the introduction of several lattice defects such as 5-fold wedge disclinations [52]. Although we have thought that the pitch of the S-layer lattice would be rather constant along the tube length, this assumption could not be confirmed in this work. This assumption was made since we know from previous work and the literature that the intrinsic curvature of the S-layer, as determined by the size of the respective bacterial cell, determines the curvature of self-assembly products in solution [53,54]. Moreover, it might also be possible that the chirality of the outer tube of the MWNTs influences the pitch of the S-layer, but previous studies with <100> and <111> silicon surfaces have shown that the S-layer did not resemble the silicon crystal structure because the ratio between the S-layer unit cell size in the 10 nm range and the lattice spacing of silicon in the 0.5 nm range was by far too large. This will be probably true for CNTs as well.

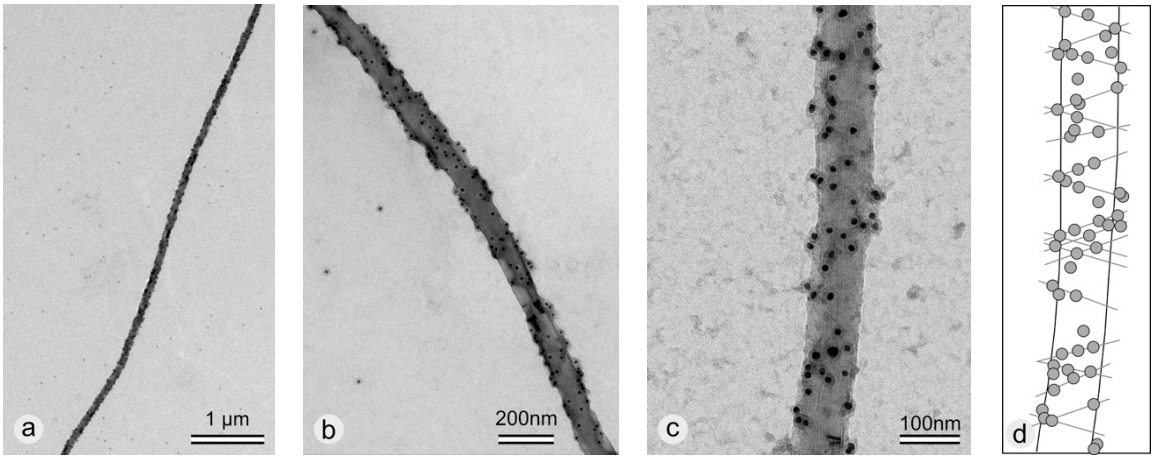



**Figure 6.** TEM images of immune gold labeled and negatively stained rSbpA$_{31\text{-}1068}$GG coated -COOH functionalized MWNTs. (**a**) The S-layer and in this was the gold nanoparticles cover tens of micrometers on the MWNT surface. (**b**,**c**) The gold particles of the gold-labeled goat antibodies can be clearly seen. It seems that they are helically arranged along the tubes as schematically shown in (**d**) for (**c**).

### *3.3. Coating of -COOH Functionalized MWNTs with rSbpA$_{31\text{-}1068}$GG Fusion Protein*

In addition to the investigation of the wild type S-layer protein (wtSbpA), -COOH functionalized MWNTs were coated with the recombinant S-layer fusion protein rSbpA$_{31\text{-}1068}$GG comprising the IgG binding region of Protein G. It could be demonstrated that also the recombinant S-layer protein coating resulted in a homogeneous distribution of the MWNTs within the buffer solution. Immune gold labeling and TEM were used to prove the general concept of functionalizing MWNTs with a tailor-made highly specific S-layer fusion protein. Gold nanoparticles, which were bound to the IgG moieties, could only be seen at the rSbpA$_{31\text{-}1068}$GG coated MWNT samples (Figure 6) while in blank experiments gold nanoparticles were not found on wtSbpA coated or uncoated MWNTs (data not shown). Moreover, it appears that the gold nanoparticles resembled the helical arrangement of the S-layer along the MWNTs (Figure 6c,d).

Although the crystalline lattice structure was not clearly visible, the immune gold labeling of the rSbpA$_{31\text{-}1068}$GG coated MWNTs confirmed the functionality of the coating. Moreover, since the IgG binding moieties were introduced at the C-terminus of the fusion protein and, in general, binding to solid supports is favored via the N-terminus, it was concluded that the rSbpA$_{31\text{-}1068}$GG was attached with its N-terminus while the C-terminus presenting the IgG binding moieties was directed towards the outside surrounding medium [29].

### *3.4. Dispersion of -COOH Functionalized MWNTs by Addition of Triton-X 100*

It has to be mentioned that we have also tried to increase the dispersibility of MWNTs by adding Triton-X 100 which immediately led to homogeneous suspensions [8]. However, it is also known that

Triton-X 100 interferes with the reassembly properties of S-layer proteins. Optimization of the protocol by lowering the Triton-X 100 concentration (below 0.01%, best with 0.003% in crystallization buffer) allowed the dispersion of -COOH functionalized MWNTs in aqueous buffer solution and—at a first glance—did not hinder the reassembly of the S-layer proteins on solid supports and MWNTs (see Supplemental Material, Figure S1). However, unfortunately, the recrystallization of wtSbpA did not occur on the surface of the MWNTs but mainly in the form of self-assembly sheets attached to the MWNTs (see Supplemental Material, Figure S2). It could not be clarified whether these self-assembly products start growing from attached S-layer proteins into the surrounding medium or whether they were detached from a loose sheathing. Therefore, the described protocol for the dispersion and S-layer coating of -COOH functionalized MWNTs—starting with ultrasonication in recrystallization buffer containing $CaCl_2$ for a total of 20 min, subsequently adding S-layer protein and continuing ultrasonication for further 4 min—was established as the standard protocol for this and future work.

## 4. Discussion

Besides chemical modifications [55], coating with synthetic polymers or surfactants [56,57], or DNA [57], also coating with proteins is seen as a promising but challenging technique to disperse and functionalize CNTs [5,9,13,36]. In general, non-covalent approaches are favored as they preserve the properties of CNTs while improving their dispersibility. The usage of BSA, DNA [58], hydrophobins [13,36], and lysozyme, which was able to disperse coated CNTs in a pH dependent way [59], was already reported. In addition, encapsulation by proteins makes CNTs not only more biocompatible but also less toxic [7,36] and offers the advantage that new functional hybrid structures with the beneficial properties of both may be developed [60]. The high surface area of CNTs and their ability to pass cell membranes make them ideal vehicles to transport drugs into cells [61,62]. Nevertheless, it has to be considered that the functionality of bound proteins may be impaired due to their random adsorption and denaturation on the CNT surface [63].

Thus, we would like to stress that the S-layer and carbon nanotube construction kit which is introduced in this work will offer the advantage to generate entirely new carriers and containers when used as catalysts, templates, scaffolds, or affinity matrices. For example, we have already shown that S-layer fusion proteins with particularly tailored bio-reactive domains allow a highly specific and sensitive (unsurpassed) functionalization of surfaces in the development of biosensor surfaces (for review see Reference [22,24]). We will make use of this knowledge and specifically bind biomolecules on native and genetically functionalized S-layer fusion protein coated MWNTs (Figure 7a). CNTs and graphene have already shown great potential in the development of biosensors due to their huge surface area, great electron transfer rate, good electrical conductivity, and ability to immobilize biologically functional molecules, such as enzymes, aptamers, or receptors [12–19]. Concerning S-layers, a considerable amount of knowledge has accumulated concerning the fabrication of amperometric sensors for glucose [64] or sucrose [65] or of optical sensors for glucose too [66]. Moreover, based on our experience in fabricating multi-enzyme amperometric biosensors, it will be possible to develop stoichiometrically well-adjusted multi-layer CNT-supported sensing layers too [65]. A promising new approach for the production of biocatalysts comprises the use of S-layer lattices that present functional multimeric enzymes on their surface, thereby forming a most accurate spatial distribution, orientation, and stability of these enzymes [67]. In comparison to conventional approaches, S-layers provide a biocompatible surface endowed with the capability to bind the functional biomolecules in a dense packing. Our approach is not limited to the use of S-layers as binding matrices only. The key feature of S-layer fusion proteins is their functional domain such as the IgG binding domain (shown in this work) [29–31], the Bet-v1 domain specific to the major birch pollen allergen [68], or for a broad range of applications the biotin binding domain [69] and affinity tag for streptavidin [70] (for review see References [22,24]). Moreover, it has to be stressed that the successful labeling of the IgG binding moieties allowed to unambiguously conclude that the S-layer was oriented with its outer face towards the medium and the biological functionality maintained—a basic requirement in our developments. In

addition, S-layer fusion proteins will allow us to perform our studies on a broader scale including material sciences when, for example, fluorescent S-layer fusion proteins with fluorescent domains (EGFP, ECFP, YFP, RFP1) or FRET pairs (Förster- or Fluorescent-resonance energy transfer) [71–73] are used. A generic approach for fluorescent proteins may be found in Reference [74]. S-layer fusion protein lattices will allow a much more specific and versatile functionalization of CNTs (Figure 7a) [69] compared to the classical approach where biomolecules are bound more-or-less randomly through diversely located functional groups (Figure 7b) [5].

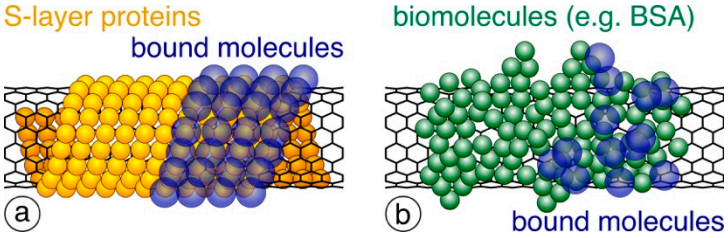



**Figure 7.** Schematic drawing of (**a**) precisely arranged S-layer proteins (shown in orange) around the CNT surface and (**b**) randomly bound biomolecules (e.g., BSA; shown in green). When used for binding further biomolecules (shown in blue), only S-layers provide a dense and precisely controlled packing.

It has to be stressed also that S-layers act as stabilizing and tethering structures and ionic reservoirs for biomembranes [75] and might provide an advantage in the development of a biomembrane based field effect transistor (FET) [76].

Moreover, tuning of the anti-fouling properties of the S-layer coating might be a further advantage for particular applications [36,77]. Alternatively, when using S-layer fusion proteins with catalytic sites exposed, a highly efficient templated biomineralization of metallic, semiconducting, or other inorganic materials will be facilitated. This might be particularly interesting for fundamental research in solid state physics, when an S-layer lattice is used as template for generating an ordered metallic nanoparticle array [78–84] directly on the CNT surface [85].

In the course of this work, it turned out that the S-layer coating increases the dispersibility of MWNTs in water dramatically, and it may be anticipated that their biocompatibility will be improved and at the same time their cytotoxicity reduced [36,57,86]. Moreover, since our TEM investigations demonstrated a good long-range order of the S-layer along the nanotubes over several (tens of) micrometers, it may be assumed that the non-classical multi stage reassembly pathway of S-layer proteins might be the key for the defect-free lattice formation over such large distances too [37–39]. Contrary to the classical approach, the multi stage process allows the healing of lattice defects in the growing crystalline domains and is pre-requisite for a self-purifying effect in the course of lattice formation [87]. Based on work with hydrophobic silicon surfaces, we assume that the healing step must be particularly favored on the highly hydrophobic surface of CNTs [45].

## 5. Summary

We would like to stress that our research, although longer term in nature, will provide technologies and materials which are more versatile to conventional approaches in the development of functional surfaces in terms of sensitivity, selectivity, and density of functional groups. Although the usage of protein coatings (e.g., BSA, lysozyme or hydrophobins) to disperse carbon nanotubes in aqueous solutions is well described in the literature, the added value of native and functionalized S-layer fusion proteins is based on their unique reassembly properties and, in this context, precisely aligned functional groups and domains for binding additional bioactive molecules and compounds.

**Supplementary Materials:** The following are available online at http://www.mdpi.com/2079-6412/9/8/492/s1, Figure S1: AFM image of wtSbpA recrystallized on a silicon wafer surface in the presence of 0.01% Triton-X 100. Although no complete protein layer could be observed, the square lattice could be easily detected, confirming the recrystallization properties in the presence of low Triton-X 100 concentrations in crystallization buffer. Figure S2:

TEM images of negatively stained wtSbpA coated MWNTs. The MWNTs had been dispersed in 0.01% Triton-X 100 before the addition of wtSbpA. The S-layer protein showed the ability to recrystallize but not by coating the MWNTs themselves but in the form of attached self-assembly products exhibiting the square lattice symmetry.

**Author Contributions:** Conceptualization, D.P., A.B., and U.B.S.; methodology, D.P., A.B., P.S., H.L., and U.B.S.; validation, D.P., A.B., and U.B.S.; formal analysis, D.P., A.B., and U.B.S.; investigation, D.P., A.B., P.S., H.L., and U.B.S.; resources, D.P.; data curation, D.P. and A.B.; writing—original draft preparation, D.P. and A.B.; writing—review and editing, D.P., A.B., P.S., H.L., and U.B.S.; visualization, D.P. and A.B.; supervision, D.P.; project administration, D.P.; funding acquisition, D.P.

**Funding:** Part of this research was funded by the Austrian Science Fund (FWF) [project P 31927-N28].

**Acknowledgments:** We would like to thank Max Willinger for his support in the preparation of MWNTs.

**Conflicts of Interest:** The authors declare no conflict of interest.

## References

1. Iijima, S. Helical Microtubules of Graphitic Carbon. *Nature* **1991**, *354*, 56–58. [CrossRef]
2. Dresselhaus, M.S.; Dresselhaus, G.; Saito, R. Physics of Carbon Nanotubes. *Carbon* **1995**, *33*, 883–891. [CrossRef]
3. Avouris, P.; Chen, Z.H.; Perebeinos, V. Carbon-based electronics. *Nat. Nanotechnol.* **2007**, *2*, 605–615. [CrossRef] [PubMed]
4. Saeed, K.; Khan, I. Carbon nanotubes-properties and applications: A review. *Carbon Lett.* **2013**, *14*, 131–144. [CrossRef]
5. Nagaraju, K.; Reddy, R.; Reddy, N. A review on protein functionalized carbon nanotubes. *J. Appl. Biomater. Func.* **2015**, *13*, E301–E312. [CrossRef]
6. Hirsch, A. Functionalization of single-walled carbon nanotubes. *Angew. Chem. Int. Ed.* **2002**, *41*, 1853–1859. [CrossRef]
7. Balasubramanian, K.; Burghard, M. Chemically functionalized carbon nanotubes. *Small* **2005**, *1*, 180–192. [CrossRef]
8. Kharissova, O.V.; Kharisov, B.I.; de Casas Ortiz, E.G. Dispersion of carbon nanotubes in water and non-aqueous solvents. *RSC Adv.* **2013**, *3*, 24812–24852. [CrossRef]
9. Calvaresi, M.; Zerbetto, F. The Devil and Holy Water: Protein and Carbon Nanotube Hybrids. *Acc. Chem. Res.* **2013**, *46*, 2454–2463. [CrossRef]
10. Posseckardt, J.; Zhang, J.W.; Mertig, M. Mobility of a supported lipid bilayer on dispersed single-walled carbon nanotubes. *Phys. Status Solidi A* **2016**, *213*, 1427–1433. [CrossRef]
11. Haft, M.; Gronke, M.; Gellesch, M.; Wurmehl, S.; Buchner, B.; Mertig, M.; Hampel, S. Tailored nanoparticles and wires of Sn, Ge and Pb inside carbon nanotubes. *Carbon* **2016**, *101*, 352–360. [CrossRef]
12. Jacobs, C.B.; Peairs, M.J.; Venton, B.J. Review: Carbon nanotube based electrochemical sensors for biomolecules. *Anal. Chim. Acta* **2010**, *662*, 105–127. [CrossRef] [PubMed]
13. Wang, X.S.; Wang, H.C.; Huang, Y.J.; Zhao, Z.X.; Qin, X.; Wang, Y.Y.; Miao, Z.Y.; Chen, Q.A.; Qiao, M.Q. Noncovalently functionalized multi-wall carbon nanotubes in aqueous solution using the hydrophobin HFBI and their electroanalytical application. *Biosens. Bioelectron.* **2010**, *26*, 1104–1108. [CrossRef] [PubMed]
14. Vashist, S.K.; Zheng, D.; Al-Rubeaan, K.; Luong, J.H.T.; Sheu, F.S. Advances in carbon nanotube based electrochemical sensors for bioanalytical applications. *Biotechnol. Adv.* **2011**, *29*, 169–188. [CrossRef] [PubMed]
15. Liu, S.; Guo, X.F. Carbon nanomaterials field-effect-transistor-based biosensors. *NPG Asia Mater.* **2012**, *4*, 1–10. [CrossRef]
16. Gomes, F.O.; Maia, L.B.; Delerue-Matos, C.; Moura, I.; Moura, J.J.G.; Morais, S. Third-generation electrochemical biosensor based on nitric oxide reductase immobilized in a multiwalled carbon nanotubes/1-n-butyl-3-methylimidazolium tetrafluoroborate nanocomposite for nitric oxide detection. *Sens. Actuators B Chem.* **2019**, *285*, 445–452. [CrossRef]
17. Kumar, S.; Bukkitgar, S.D.; Singh, S.; Singh, V.; Reddy, K.R.; Shetti, N.P.; Reddy, C.V.; Sadhu, V.; Naveen, S. Electrochemical Sensors and Biosensors Based on Graphene Functionalized with Metal Oxide Nanostructures for Healthcare Applications. *Chemistryselect* **2019**, *4*, 5322–5337. [CrossRef]

18. Kwon, O.S.; Song, H.S.; Park, T.H.; Jang, J. Conducting Nanomaterial Sensor Using Natural Receptors. *Chem. Rev.* **2019**, *119*, 36–93. [CrossRef]
19. Wayu, M.B.; Pannell, M.J.; Labban, N.; Case, W.S.; Pollock, J.A.; Leopold, M.C. Functionalized carbon nanotube adsorption interfaces for electron transfer studies of galactose oxidase. *Bioelectrochemistry* **2019**, *125*, 116–126. [CrossRef]
20. Pantarotto, D.; Singh, R.; McCarthy, D.; Erhardt, M.; Briand, J.P.; Prato, M.; Kostarelos, K.; Bianco, A. Functionalized carbon nanotubes for plasmid DNA gene delivery. *Angew. Chem. Int. Ed.* **2004**, *43*, 5242–5246. [CrossRef]
21. Jovanovic, S.P.; Markovic, Z.M.; Kleut, D.N.; Romcevic, N.Z.; Trajkovic, V.S.; Dramicanin, M.D.; Markovic, B.M.T. A novel method for the functionalization of gamma-irradiated single wall carbon nanotubes with DNA. *Nanotechnology* **2009**, *20*. [CrossRef] [PubMed]
22. Sleytr, U.B.; Schuster, B.; Egelseer, E.M.; Pum, D. S-layers: Principles and applications. *FEMS Microbiol. Rev.* **2014**, *38*, 823–864. [CrossRef] [PubMed]
23. Pum, D.; Sleytr, U.B. Reassembly of S-layer proteins. *Nanotechnology* **2014**, *25*, 312001. [CrossRef] [PubMed]
24. Egelseer, E.M.; Ilk, N.; Pum, D.; Messner, P.; Schäffer, C.; Schuster, B.; Sleytr, U.B. S-Layers, microbial, biotechnological applications. In *Encyclopedia of Industrial Biotechnology: Bioprocess, Bioseparation, and Cell Technology*; Flickinger, M.C., Ed.; John Wiley and Sons: Hoboken, NJ, USA, 2010; Volume 7, pp. 4424–4448.
25. Sleytr, U.B. Self-assembly of the hexagonally and tetragonally arranged subunits of bacterial surface layers and their reattachment to cell walls. *J. Ultrastruct. Res.* **1976**, *55*, 360–377. [CrossRef]
26. Ladenhauf, E.M.; Pum, D.; Wastl, D.S.; Toca-Herrera, J.L.; Phan, N.V.H.; Lieberzeit, P.A.; Sleytr, U.B. S-layer based biomolecular imprinting. *RSC Adv.* **2015**, *5*, 83558–83564. [CrossRef]
27. Schuster, D.; Kupcu, S.; Belton, D.J.; Perry, C.C.; Stoger-Pollach, M.; Sleytr, U.B.; Pum, D. Construction of silica-enhanced S-layer protein cages. *Acta Biomater.* **2013**, *9*, 5689–5697. [CrossRef]
28. Ilk, N.; Egelseer, E.M.; Sleytr, U.B. S-layer fusion proteins—Construction principles and applications. *Curr. Opin. Biotechnol.* **2011**, *22*, 824–831. [CrossRef]
29. Völlenkle, C.; Weigert, S.; Ilk, N.; Egelseer, E.; Weber, V.; Loth, F.; Falkenhagen, D.; Sleytr, U.B.; Sara, M. Construction of a functional S-layer fusion protein comprising an immunoglobulin G-binding domain for development of specific adsorbents for extracorporeal blood purification. *Appl. Environ. Microbiol.* **2004**, *70*, 1514–1521. [CrossRef]
30. Ucisik, M.H.; Küpcü, S.; Breitwieser, A.; Gelbmann, N.; Schuster, B.; Sleytr, U.B. S-layer fusion protein as a tool functionalizing emulsomes and CurcuEmulsomes for antibody binding and targeting. *Colloids Surf. B* **2015**, *128*, 132–139. [CrossRef]
31. Breitwieser, A.; Pum, D.; Toca-Herrera, J.L.; Sleytr, B.U. Magnetic beads functionalized with recombinant S-layer protein exhibit high human IgG-binding and anti-fouling properties. *Curr. Top. Pept. Protein Res.* **2016**, *17*, 45–55.
32. Scheicher, S.R.; Kainz, B.; Kostler, S.; Reitinger, N.; Steiner, N.; Ditlbacher, H.; Leitner, A.; Pum, D.; Sleytr, U.B.; Ribitsch, V. 2D crystalline protein layers as immobilization matrices for the development of DNA microarrays. *Biosens. Bioelectron.* **2013**, *40*, 32–37. [CrossRef]
33. Pum, D.; Sleytr, U.B. Large-scale reconstruction of crystalline bacterial surface layer proteins at the air-water interface and on lipids. *Thin Solid Films* **1994**, *244*, 882–886. [CrossRef]
34. Ilk, N.; Vollenkle, C.; Egelseer, E.M.; Breitwieser, A.; Sleytr, U.B.; Sara, M. Molecular characterization of the S-layer gene, sbpA, of Bacillus sphaericus CCM 2177 and production of a functional S-layer fusion protein with the ability to recrystallize in a defined orientation while presenting the fused allergen. *Appl. Environ. Microb.* **2002**, *68*, 3251–3260. [CrossRef]
35. Pavkov-Keller, T.; Howorka, S.; Keller, W. The structure of bacterial S-layer proteins. *Prog. Mol. Biol. Transl. Sci.* **2011**, *103*, 73–130. [CrossRef]
36. Yang, W.; Ren, Q.; Wu, Y.N.; Morris, V.K.; Rey, A.A.; Braet, F.; Kwan, A.H.; Sunde, M. Surface functionalization of carbon nanomaterials by self-assembling hydrophobin proteins. *Biopolymers* **2013**, *99*, 84–94. [CrossRef]
37. Chung, S.; Shin, S.H.; Bertozzi, C.R.; De Yoreo, J.J. Self-catalyzed growth of S layers via an amorphous-to-crystalline transition limited by folding kinetics. *Proc. Natl. Acad. Sci. USA* **2010**, *107*, 16536–16541. [CrossRef]

38. Shin, S.H.; Chung, S.; Sanii, B.; Comolli, L.R.; Bertozzi, C.R.; De Yoreo, J.J. Direct observation of kinetic traps associated with structural transformations leading to multiple pathways of S-layer assembly. *Proc. Natl. Acad. Sci. USA* **2012**, *109*, 12968–12973. [CrossRef]
39. Breitwieser, A.; Iturri, J.; Toca-Herrera, J.L.; Sleytr, U.B.; Pum, D. In Vitro Characterization of the Two-Stage Non-Classical Reassembly Pathway of S-Layers. *Int. J. Mol. Sci.* **2017**, *18*, 400. [CrossRef]
40. Pum, D.; Sleytr, U.B. Anisotropic crystal growth of the S-layer of Bacillus sphaericus CCM 2177 at the air/water interface. *Colloids Surf. A* **1995**, *102*, 99–104. [CrossRef]
41. Baranova, E.; Fronzes, R.; Garcia-Pino, A.; Van Gerven, N.; Papapostolou, D.; Pehau-Arnaudet, G.; Pardon, E.; Steyaert, J.; Howorka, S.; Remaut, H. SbsB structure and lattice reconstruction unveil $Ca^{2+}$ triggered S-layer assembly. *Nature* **2012**, *487*, 119–122. [CrossRef]
42. Rad, B.; Haxton, T.K.; Shon, A.; Shin, S.H.; Whitelam, S.; Ajo-Franklin, C.M. Ion-specific control of the self-assembly dynamics of a nanostructured protein lattice. *ACS Nano* **2015**, *9*, 180–190. [CrossRef] [PubMed]
43. Ilk, N.; Kosma, P.; Puchberger, M.; Egelseer, E.M.; Mayer, H.F.; Sleytr, U.B.; Sára, M. Structural and functional analyses of the secondary cell wall polymer of *Bacillus sphaericus* CCM 2177 that serves as an S-layer-specific anchor. *J. Bacteriol.* **1999**, *181*, 7643–7646. [PubMed]
44. Egelseer, E.M.; Leitner, K.; Jarosch, M.; Hotzy, C.; Zayni, S.; Sleytr, U.B.; Sára, M. The S-layer proteins of two *Bacillus stearothermophilus* wild-type strains are bound via their N-terminal region to a secondary cell wall polymer of identical chemical composition. *J. Bacteriol.* **1998**, *180*, 1488–1495. [PubMed]
45. Györvary, E.S.; Stein, O.; Pum, D.; Sleytr, U.B. Self-assembly and recrystallization of bacterial S-layer proteins at silicon supports imaged in real time by atomic force microscopy. *J. Microsc.* **2003**, *212*, 300–306. [CrossRef] [PubMed]
46. Singer, G.; Siedlaczek, P.; Sinn, G.; Rennhofer, H.; Micusik, M.; Omastova, M.; Unterlass, M.M.; Wendrinsky, J.; Milotti, V.; Fedi, F.; et al. Acid Free Oxidation and Simple Dispersion Method of MWCNT for High-Performance CFRP. *Nanomaterials* **2018**, *8*, 912. [CrossRef] [PubMed]
47. Schneider, C.A.; Rasband, W.S.; Eliceiri, K.W. NIH Image to ImageJ: 25 years of image analysis. *Nat. Methods* **2012**, *9*, 671–675. [CrossRef]
48. Yang, X.S.; Lee, J.; Yuan, L.X.; Chae, S.R.; Peterson, V.K.; Minett, A.I.; Yin, Y.B.; Harris, A.T. Removal of natural organic matter in water using functionalised carbon nanotube buckypaper. *Carbon* **2013**, *59*, 160–166. [CrossRef]
49. Harris, W.F. Disclinations. *Sci. Am.* **1977**, *237*, 130–145. [CrossRef]
50. DeRosier, D.J.; Moore, P.B. Reconstruction of 3-Dimensional Images from Electron Micrographs of Structures with Helical Symmetry. *J. Mol. Biol.* **1970**, *52*, 355–369. [CrossRef]
51. Diaz, R.; Rice, W.J.; Stokes, D.L. Fourier-Bessel Reconstruction of Helical Assemblies. *Methods Enzymol.* **2010**, *482*, 131–165. [CrossRef]
52. Messner, P.; Pum, D.; Sára, M.; Stetter, K.O.; Sleytr, U.B. Ultrastructure of the cell envelope of the archaebacteria Thermoproteus tenax and Thermoproteus neutrophilus. *J. Bacteriol.* **1986**, *166*, 1046–1054. [CrossRef] [PubMed]
53. Messner, P.; Pum, D.; Sleytr, U.B. Characterization of the ultrastructure and the self-assembly of the surface layer of Bacillus stearothermophilus strain NRS 2004/3a. *J. Ultrastruct. Mol. Struct. Res.* **1986**, *97*, 73–88. [CrossRef]
54. Bobeth, M.; Blecha, A.; Bluher, A.; Mertig, M.; Korkmaz, N.; Ostermann, K.; Rodel, G.; Pompe, W. Formation of tubes during self-assembly of bacterial surface layers. *Langmuir* **2011**, *27*, 15102–15111. [CrossRef] [PubMed]
55. Ali-Boucetta, H.; Nunes, A.; Sainz, R.; Herrero, M.A.; Tian, B.; Prato, M.; Bianco, A.; Kostarelos, K. Asbestos-like pathogenicity of long carbon nanotubes alleviated by chemical functionalization. *Angew. Chem. Int. Ed.* **2013**, *52*, 2274–2278. [CrossRef] [PubMed]
56. Rastogi, R.; Kaushal, R.; Tripathi, S.K.; Sharma, A.L.; Kaur, I.; Bharadwaj, L.M. Comparative study of carbon nanotube dispersion using surfactants. *J. Colloid Interface Sci.* **2008**, *328*, 421–428. [CrossRef] [PubMed]
57. Mallakpour, S.; Soltanian, S. Surface functionalization of carbon nanotubes: Fabrication and applications. *RSC Adv.* **2016**, *6*, 109916–109935. [CrossRef]
58. Awasthi, K.; Singh, D.P.; Singh, S.; Dash, D.; Srivastava, O.N. Attachment of biomolecules (protein and DNA) to amino-functionalized carbon nanotubes. *New Carbon Mater.* **2009**, *24*, 301–306. [CrossRef]

59. Nepal, D.; Geckeler, K.E. pH-sensitive dispersion and debundling of single-walled carbon nanotubes: Lysozyme as a tool. *Small* **2006**, *2*, 406–412. [CrossRef]
60. Zhang, Y.J.; Li, J.; Shen, Y.F.; Wang, M.J.; Li, J.H. Poly-L-lysine functionalization of single-walled carbon nanotubes. *J. Phys. Chem. B* **2004**, *108*, 15343–15346. [CrossRef]
61. Liu, Z.; Robinson, J.T.; Tabakman, S.M.; Yang, K.; Dai, H.J. Carbon materials for drug delivery & cancer therapy. *Mater. Today* **2011**, *14*, 316–323. [CrossRef]
62. Lacerda, L.; Raffa, S.; Prato, M.; Bianco, A.; Kostarelos, K. Cell-penetrating CNTs for delivery of therapeutics. *Nano Today* **2007**, *2*, 38–43. [CrossRef]
63. Butler, J.E.; Ni, L.; Brown, W.R.; Joshi, K.S.; Chang, J.; Rosenberg, B.; Voss, E.W., Jr. The immunochemistry of sandwich ELISAs–VI. Greater than 90% of monoclonal and 75% of polyclonal anti-fluorescyl capture antibodies (CAbs) are denatured by passive adsorption. *Mol. Immunol.* **1993**, *30*, 1165–1175. [CrossRef]
64. Neubauer, A.; Pum, D.; Sleytr, U.B. An Amperometric Glucose Sensor-Based on Isoporous Crystalline Protein Membranes as Immobilization Matrix. *Anal. Lett.* **1993**, *26*, 1347–1360. [CrossRef]
65. Neubauer, A.; Hodl, C.; Pum, D.; Sleytr, U.B. A Multistep Enzyme Sensor for Sucrose Based on S-Layer Microparticles as Immobilization Matrix. *Anal. Lett.* **1994**, *27*, 849–865. [CrossRef]
66. Neubauer, A.; Pum, D.; Sleytr, U.B.; Klimant, I.; Wolfbeis, O.S. Fibre-optic glucose biosensor using enzyme membranes with 2-D crystalline structure. *Biosens. Bioelectron.* **1996**, *11*, 317–325. [CrossRef]
67. Ferner-Ortner-Bleckmann, J.; Gelbmann, N.; Tesarz, M.; Egelseer, E.M.; Sleytr, U.B. Surface-layer lattices as patterning element for multimeric extremozymes. *Small* **2013**, *9*, 3887–3894. [CrossRef] [PubMed]
68. Breitwieser, A.; Egelseer, E.M.; Moll, D.; Ilk, N.; Hotzy, C.; Bohle, B.; Ebner, C.; Sleytr, U.B.; Sara, M. A recombinant bacterial cell surface (S-layer)-major birch pollen allergen-fusion protein (rSbsC/Bet v1) maintains the ability to self-assemble into regularly structured monomolecular lattices and the functionality of the allergen. *Protein Eng.* **2002**, *15*, 243–249. [CrossRef]
69. Moll, D.; Huber, C.; Schlegel, B.; Pum, D.; Sleytr, U.B.; Sara, M. S-layer-streptavidin fusion proteins as template for nanopatterned molecular arrays. *Proc. Natl. Acad. Sci. USA* **2002**, *99*, 14646–14651. [CrossRef]
70. Huber, C.; Liu, J.; Egelseer, E.M.; Moll, D.; Knoll, W.; Sleytr, U.B.; Sara, M. Heterotetramers formed by an S-layer-streptavidin fusion protein and core-streptavidin as a nanoarrayed template for biochip development. *Small* **2006**, *2*, 142–150. [CrossRef]
71. Kainz, B.; Steiner, K.; Moller, M.; Pum, D.; Schaffer, C.; Sleytr, U.B.; Toca-Herrera, J.L. Absorption, steady-state fluorescence, fluorescence lifetime, and 2D self-assembly properties of engineered fluorescent S-layer fusion proteins of Geobacillus stearothermophilus NRS 2004/3a. *Biomacromolecules* **2010**, *11*, 207–214. [CrossRef]
72. Kainz, B.; Steiner, K.; Sleytr, U.B.; Pum, D.; Toca-Herrera, J.L. Fluorescence energy transfer in the bi-fluorescent S-layer tandem fusion protein ECFP-SgsE-YFP. *J. Struct. Biol.* **2010**, *172*, 276–283. [CrossRef] [PubMed]
73. Kainz, B.; Steiner, K.; Sleytr, U.B.; Pum, D.; Toca-Herrera, J.L. Fluorescent S-layer protein colloids. *Soft Matter* **2010**, *6*, 3809–3814. [CrossRef]
74. Dunakey, S.J.G.; Coyle, B.L.; Thomas, A.; Xu, M.; Swift, B.J.F.; Baneyx, F. Selective Labeling and Decoration of the Ends and Sidewalls of Single-Walled Carbon Nanotubes Using Mono- and Bispecific Solid-Binding Fluorescent Proteins. *Bioconjugate Chem.* **2019**, *30*, 959–965. [CrossRef] [PubMed]
75. Schuster, B.; Sleytr, U.B. Composite S-layer lipid structures. *J. Struct. Biol.* **2009**, *168*, 207–216. [CrossRef]
76. Gong, H.; Chen, F.; Huang, Z.L.; Gu, Y.; Zhang, Q.Z.; Chen, Y.J.; Zhang, Y.; Zhuang, J.; Cho, Y.K.; Fang, R.N.H.; et al. Biomembrane-Modified Field Effect Transistors for Sensitive and Quantitative Detection of Biological Toxins and Pathogens. *ACS Nano* **2019**, *13*, 3714–3722. [CrossRef]
77. Rothbauer, M.; Küpcü, S.; Sticker, D.; Sleytr, U.B.; Ertl, P. Exploitation of S-layer Anisotropy: pH-dependent Nanolayer Orientation for Cellular Micropatterning. *ACS Nano* **2013**, *7*, 8020–8030. [CrossRef]
78. Shenton, W.; Pum, D.; Sleytr, U.B.; Mann, S. Biocrystal templating of CdS superlattices using self-assembled bacterial S-layers. *Nature* **1997**, *389*, 585–587. [CrossRef]
79. Dieluweit, S.; Pum, D.; Sleytr, U.B. Formation of a gold superlattice on an S-layer with square lattice symmetry. *Supramol. Sci.* **1998**, *5*, 15–19. [CrossRef]
80. Mertig, M.; Kirsch, R.; Pompe, W.; Engelhardt, H. Fabrication of highly oriented nanocluster arrays by biomolecular templating. *Eur. Phys. J. D* **1999**, *9*, 45–48. [CrossRef]
81. Pompe, W.; Mertig, M.; Kirsch, R.; Wahl, R.; Ciacchi, L.C.; Richter, J.; Seidel, R.; Vinzelberg, H. Formation of metallic nanostructures on biomolecular templates. *Zeitschrift Fur Metallkunde* **1999**, *90*, 1085–1091.

82. Mertig, M.; Wahl, R.; Lehmann, M.; Simon, P.; Pompe, W. Formation and manipulation of regular metallic nanoparticle arrays on bacterial surface layers: An advanced TEM study. *Eur. Phys. J. D* **2001**, *16*, 317–320. [CrossRef]
83. Queitsch, U.; Mohn, E.; Schaffel, F.; Schultz, L.; Rellinghaus, B.; Bluher, A.; Mertig, M. Regular arrangement of nanoparticles from the gas phase on bacterial surface-protein layers. *Appl. Phys. Lett.* **2007**, *90*, 113114. [CrossRef]
84. Mann, S. Self-assembly and transformation of hybrid nano-objects and nanostructures under equilibrium and non-equilibrium conditions. *Nat. Mater.* **2009**, *8*, 781–792. [CrossRef]
85. Grigoryan, G.; Kim, Y.H.; Acharya, R.; Axelrod, K.; Jain, R.M.; Willis, L.; Drndic, M.; Kikkawa, J.M.; DeGrado, W.F. Computational design of virus-like protein assemblies on carbon nanotube surfaces. *Science* **2011**, *332*, 1071–1076. [CrossRef]
86. Vardharajula, S.; Ali, S.Z.; Tiwari, P.M.; Eroglu, E.; Vig, K.; Dennis, V.A.; Singh, S.R. Functionalized carbon nanotubes: Biomedical applications. *Int. J. Nanomed.* **2012**, *7*, 5361–5374. [CrossRef]
87. Sleutel, M.; Van Driessche, A.E.S. Role of clusters in nonclassical nucleation and growth of protein crystals. *Proc. Natl. Acad. Sci. USA* **2014**, *111*, E546–E553. [CrossRef]




© 2019 by the authors. Licensee MDPI, Basel, Switzerland. This article is an open access article distributed under the terms and conditions of the Creative Commons Attribution (CC BY) license (http://creativecommons.org/licenses/by/4.0/).